



<http://researchspace.auckland.ac.nz>

ResearchSpace@Auckland

Copyright Statement

The digital copy of this thesis is protected by the Copyright Act 1994 (New Zealand).

This thesis may be consulted by you, provided you comply with the provisions of the Act and the following conditions of use:

- Any use you make of these documents or images must be for research or private study purposes only, and you may not make them available to any other person.
- Authors control the copyright of their thesis. You will recognise the author's right to be identified as the author of this thesis, and due acknowledgement will be made to the author where appropriate.
- You will obtain the author's permission before publishing any material from their thesis.

To request permissions please use the Feedback form on our webpage.

<http://researchspace.auckland.ac.nz/feedback>

General copyright and disclaimer

In addition to the above conditions, authors give their consent for the digital copy of their work to be used subject to the conditions specified on the Library Thesis Consent Form.

STRUCTURE OF THE BROADLANDS-OHAAKI
GEOHERMAL FIELD (NEW ZEALAND)
BASED ON INTERPRETATION OF SEISMIC AND
GRAVITY DATA

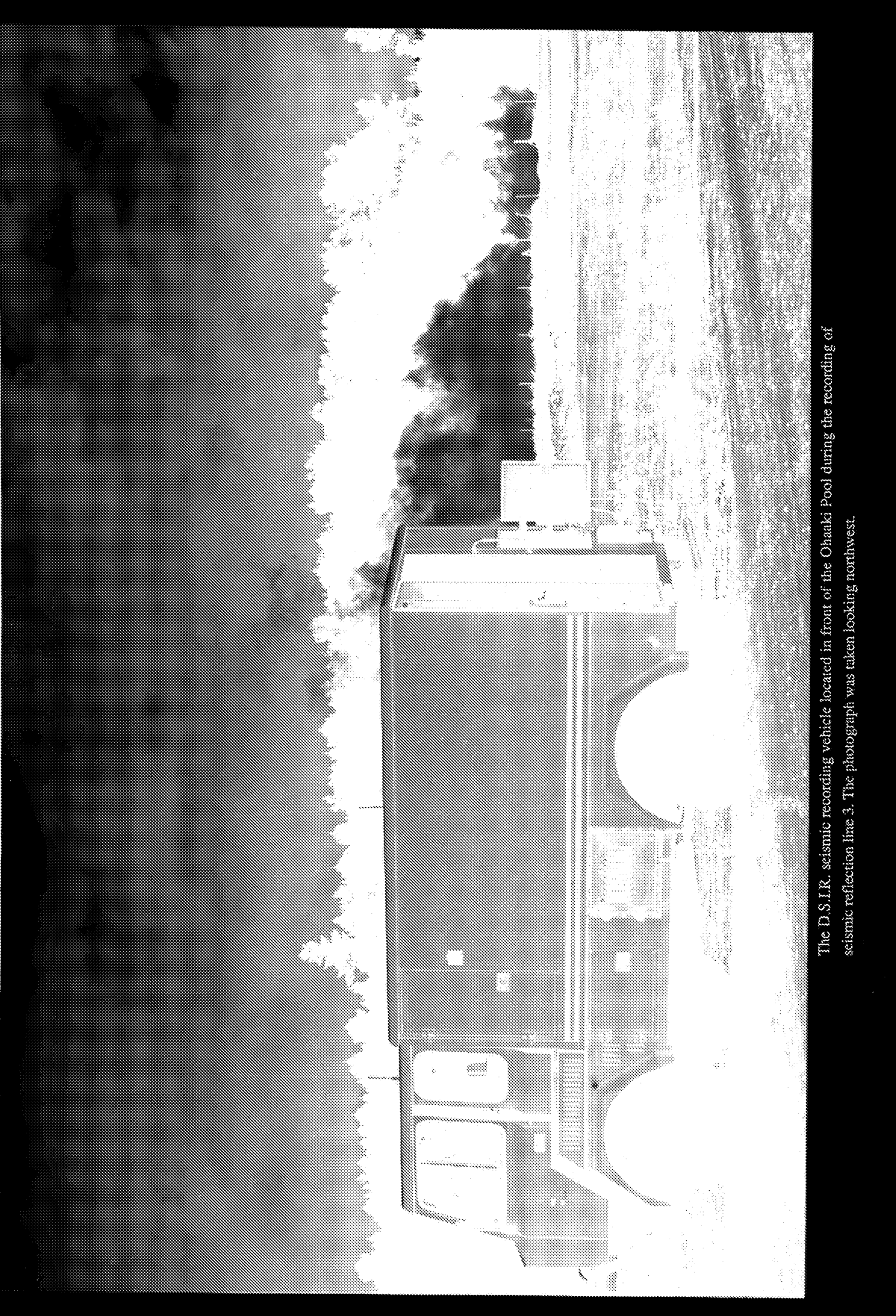
by

Stuart Henrys

A thesis presented to University of Auckland in fulfilment of the requirements for
the degree of
Doctor of Philosophy in Geology.

November 1987

This thesis is dedicated to Estelle and Lorraine who have sacrificed the most and can still smile.



The D.S.I.R. seismic recording vehicle located in front of the Ohaaki Pool during the recording of seismic reflection line 3. The photograph was taken looking northwest.

Abstract

The structure of the Broadlands-Ohaaki hot water geothermal field has been studied by analysis of seismic and gravity data.

The 1984 seismic survey provided 26 km of multifold (12-fold) reflection data and refraction data (up to 1 km) along 6 profiles in the vicinity of the geothermal field. Test data were acquired along 2 profiles of 1 km length and included a walk-away noise spread. An attempt was also made to record shear-waves (SV) along one profile with in-line horizontal geophones. Processing of reflection data indicated the importance of static corrections, velocity filtering and spectral balancing of the trace amplitude spectrum before deconvolution.

Delay times from the analysis of refracted (first) arrivals outline areas of anomalous low velocity that coincide with areas of highest surface temperatures ($>50^{\circ}\text{C}$ at 15 m depth). Ray trace modelling of travel times near the Ohaaki Pool delineate an anomalously low-velocity zone to a depth of 200 m. The frequency and amplitude of the recorded signals near the Ohaaki Pool are attenuated in comparison to field records from outside areas with high surface temperatures. Converted shear-waves indicate that Poisson's ratio is low (0.17 to 0.20) in this area. These effects are consistent with a steam/water zone occurring close to the surface

Common-mid-point derived velocities and ray-tracing inversion of reflecting horizons were used to determine the 3-dimensional velocity distribution beneath the geothermal field. A low-velocity zone, in which velocities are 10-20% lower inside the geothermal field, coincides with the region of highest signal attenuation ($Q < 20$), the productive borefield, and the region of highest fluid temperature ($>250^{\circ}\text{C}$ at 1000 m depth)

The seismic stratigraphy of the volcanic units was established using drill hole data and synthetic seismograms. The top and bottom of the Ohaaki Rhyolite and Broadlands Dacite account for the major reflecting horizons with occasional less strong reflections from the top of the Rangitaiki Ignimbrite. However, even strong reflectors are not coherent across any single section and the top of the rhyolite and dacite flows may show up with strong reflections at one part of the profile, but elsewhere with weak or no reflections. The limited success in enhancing signal quality below 500-700 m depth is attributed to a combination of noise generated in the low velocity surface layer and the complexity of the geological structure at depth.

Analysis of noise characteristics of the Broadlands-Ohaaki reflection data included computation of synthetic seismograms and spectral analysis of recorded seismograms. Theoretical modelling of near-surface structures showed that prominent low-frequency noise trains observed in field data are due to waves trapped in the surface layer that are excited by direct waves from shallow (5-10 m) shots. A very rapid increase in seismic wavespeed occurs at the water table and causes the surface layer to act as a waveguide which traps low-

frequency Rayleigh waves and air-coupled Rayleigh waves visible on near offset traces. Compressional energy is also efficiently converted into shear-waves (SV) and is dominant as reverberating reflected refracted energy at far offsets (>400 m). In addition, there is resonant coupling between the surface waves and multiple reflections. Surface-consistent spectral analysis indicates that variation in receiver response is a function of the thickness of the low-velocity layer.

Reinterpretation of refraction data (1968 survey) by ray-trace modelling elucidated new structural and stratigraphic details which tie in with well data and confirms the velocity structure established from reflection data. Near offset refracted arrivals clearly define the top of the Ohaaki Rhyolite (2200-2800 m/sec) in the western part of the field and the top of the Broadlands Dacite (2650-3200 m/sec) in the east. Longer offset (>3 km) travel times could be modelled as arrivals from the top of the Rautawiri Breccia and Rangitaiki Ignimbrite (velocities between 2800 m/sec and 3800 m/sec). Arrivals from greywacke basement (4500 m/sec) could only be detected in the east outside the geothermal field coming from depths less than 1.0 km.

A 3-dimensional interpretation of residual gravity anomalies was also attempted since the seismic sections and detailed well data provide strong constraints. Isodensity and isoporosity contours of the Rautawiri Breccia, Waiora Formation and the Ohaaki Rhyolite reveal areas of high density and low porosity corresponding to the productive regions of the borefield. This density increase is caused by alteration and mineralisation.

The detailed interpretation models allow the construction of basement contour and isopach maps. Basement structural-contours show that the basement surface is very complex with significant vertical displacement along a series of predominantly northwest-southeast trending normal faults of limited horizontal extent and with no evidence of significant cross faulting. The basement reaches a maximum depth of 2300 m b.s.l west of the geothermal field. East of the geothermal field the basement rises along a series of northeast-southwest trending normal faults including the Kaingaroa Fault. Isopachs of the productive Rautawiri Breccia and Waiora Formation indicate that the thickest sequence of these units lies to the north and south of the geothermal field apart from at least two structurally controlled depressions inside the field where the thickness of the Rautawiri Breccia is greater than 500 m. Elsewhere, the combined total thickness of these units is less than 400 m.

The Broadlands Dacite dome extends over an area of about 16 km². A magnetic high associated with the Broadlands Dacite is caused by the unaltered, normally magnetised dacite east of the resistivity boundary. Isopachs of the Ohaaki Rhyolite indicate that its thickness increases to the northwest. This finding cannot be reconciled with an earlier concept of a localised Ohaaki dome structure which required a localised feeder dyke within the field. The Ohaaki Rhyolite is probably part of a more extensive chain of rhyolites outcropping to the north and west.

Acknowledgements

The Broadlands-Ohaaki seismic reflection experiment has depended on the support and assistance of many people.

Firstly I wish to thank my supervisors Associate Professor M.P. Hochstein and Dr J. Cassidy. I also thank Associate Professor A.R. Levander (Rice University) and Dr B.J. Brennan (Physics Department, A.U.) who acted as unofficial supervisors in specialists fields. Thanks must also go to Dr T. Hatherton (Geophysics Division, D.S.I.R.) for his enthusiastic support at the start of this project and to the staff at Geophysics Division for their cooperation throughout.

This work was carried out while the author was in receipt of a Postgraduate Scholarship from the University Grants Committee and the McKee Trust Postgraduate Scholarship. I also thank the Fulbright Hayes Foundation for a grant to travel to the U.S.. I am very grateful to the staff at Rice University, Houston, including the Chairman Professor A.W. Bally, Associate Professor A.R. Levander, B. Gibson, and Associate Professor R. Hill for their help and support. Financial assistance was also provided by the University Grants Committee (grants 392166 and 423008) and Electrocorp (formally Electricity Division of the Ministry of Energy).

Landowners and farmers in the Broadlands-Ohaaki area have been very cooperative and formal land clearance issued by the following people and authorities ^{LS} are acknowledged:

- a) G. Gay of the Ministry of Works and Development (MWD),
- b) T.B. Nikora of the Ngati Tahu Tribal Trust,
- c) D.R. Marshall of the Department of Lands and Survey (Rotorua),
- d) J. Kohi of Deep Creek Land Settlement,
- e) Waikato Valley Authority,
- f) Zanpro Ltd.,
- g) and the following farmers; C.R. Whiteman, R.J. Lindsay, R. Wells, Mr Thornburrow, A.L. Tompkins, Mr Frampton, and Mr Johnson.

For field assistance I am indebted to the Geophysics Division (D.S.I.R.) seismic crew including L. Carrington, C. O'Reilly, and A. Hefford and drillers D. Clemence and B. Robson. K. Youngman, R. Anstiss, V. Coothongkul, T. Cowbourne, C. Yong, Dr J. Cassidy and E. Anderson also helped. I thank S. Jolly of the MWD for supplying survey

markers and help with tacheometry. For the use of facilities at Wairakei, I thank Dr T. Hunt and the scientists at the Geothermal Research Centre (D.S.I.R.). Comfortable accommodation was made available at the New Zealand Electricity Division Hostel at Wairakei for 2 months and for this I am grateful to T. Cottle and his staff.

Other University departments have contributed. The Geography department (Dr D. Hawke) kindly allowed me to use the digitiser on a number of occasions and the Computer Centre staff 'punched' many hundreds of lines of code into computer files and assisted with program development. Staff and students at the Geothermal Institute donated many hours of their time and patience to meet my demands.

This project has been enhanced by the help of several other institutions and I am grateful for the advice and assistance of Dr D. Woodward, Dr J. Haines, Dr. T. Hunt, and T.C. Mumme (Geophysics Division, D.S.I.R.), Dr G. Grindley (Geological Survey, D.S.I.R.), Dr T. Mahon (GENZL), L. Chapman and N. Fitzgerald (Geophysical Company of Norway, Wellington), Dr D. Lawton (Calgary University, Canada) and Dr S. Ehara (Kyushu University, Japan). Dr A. Carmen of Geophysics Division kindly helped with reduction of gravity data and supplied me a copy of D.S.I.R. network gravity data for the greater Broadlands-Ohaaki region. P. Bixley (formally MWD) supplied sonic logs from Wairakei wells. Dr F. Hilterman (Geophysical Development Corporation) made available the "SOLID" program for computing synthetic seismograms. Prof. R. Gutdeutsch (Institut für Meteorologie und Geophysik der Universität Wien) kindly supplied me with an early version of the basic ray-tracing program. Mr T. Mills of Electrocorp assisted in acquiring financial support while I was in Houston.

In preparation of the manuscript I also acknowledge Dr P. Browne for comments on geological chapters, E. Leaming for assistance in the Geology Department library, and R Harris for help with draughting. In addition I would like to thank K. Youngman, A. Absar, G. Scott, S. Soengkono, and T. Hagdu for extended lunchtime discussions.

Finally, I would like to thank my parents for encouragement in this study and most of all I thank my wife and daughter, Estelle and Lorraine for their perseverance throughout.

Contents

Title	i
Dedication	ii
Front piece	iii
Abstract	iv
Acknowledgements	vi
Contents	viii
List of Tables	xiii
List of Figures	xiv
Contents of Map Pocket	xxiii

Chapter 1. Introduction

1.1	Introduction	1
1.2	Seismic Reflection Profiling	2
1.3	Seismic Reflection Investigations of Geothermal Fields	5
1.4	Outline of Thesis	9

Chapter 2. The Broadlands-Ohaaki Geothermal Field

2.1	Introduction	11
2.2	Taupo Volcanic Zone	11
2.3	Geology and Geophysics	16
2.4	Hydrology	28
2.5	Summary	29

**Chapter 3. Compressional-Wave Velocity and
Attenuation in an Idealised Geothermal Hot
Water Reservoir.**

3.1	Introduction	33
3.2	Relaxed and Unrelaxed Bulk Modulus	35
3.3	Calculation of Synthetic Seismograms	41
3.3.1	The Effect of Temperature (Pore Fluid=hot water)	47
3.3.2	Two-Phase System (Pore Fluid=Mixture of Hot Water and Steam)	47
3.4	Conclusion	52

Chapter 4. Seismic Reflection Data Acquisition

4.1	Introduction	53
4.2	Broadlands-Ohaaki Seismic Reflection Survey	55
4.3	Seismic Reflection Field Tests	55
4.3.1	Walk-Away Noise Test	57
4.3.2	Multiple versus Single Geophones	62
4.3.3	Geophone Spread Geometry	66
4.3.4	Charge Size Study	71
4.3.5	Shot Depth Study	71
4.3.6	Shear Waves	74
4.4	Main Reflection Survey	78

Chapter 5. Seismic Reflection Data Processing

5.1	Introduction	83
5.2	Data Quality	85
5.3	Processing Sequence	89
5.3.1	Demultiplex and Geometry	89
5.3.2	Editing	91
5.3.3	Spherical Divergence Correction and Trace Amplitude Balancing	91
5.3.4	Datum Statics	92
5.3.5	Frequency-Wavenumber Filtering	99
5.3.6	Spectral Balancing and Deconvolution	101
5.3.7	Common-Mid-Point (CMP) Sorting	107
5.3.8	Velocity Analysis and Normal Moveout correction (NMO)	107

5.3.9	Mute	110
5.3.10	Stack	110
5.3.11	Residual Statics	115
5.3.12	Velocity Analysis, Final Stack, and 2nd Pass Residual Statics	115
5.3.13	Migration	118
5.3.14	Time Variant Filtering	118
5.4	True Amplitude Processing	121
5.5	Discussion	121
5.6	Conclusions	123

Chapter 6. Near-Surface Seismic Wave Propagation Effects

6.1	Introduction	125
6.2	Observations of Field Records	127
6.3	Walk-Away Noise Test	127
6.4	Theoretical Modelling of Walk-Away Test Data	133
6.5	Finite-Difference Modelling of Walk-Away Test Data	140
6.6	Comparison of Finite Difference Synthetic Seismograms with Field Data	143
6.7	Surface-Consistent Spectral Analysis	147
6.8	Surface-Consistent Filtering	153
6.9	Recommendations and Future Seismic Reflection Surveys in the TVZ	158
6.10	Conclusions	160

Chapter 7. Interpretation of Seismic Reflection Data over the Broadlands-Ohaaki Geothermal Field

7.1	Introduction	163
7.2	Seismic Character of Reflections	164
7.3	Detailed Velocity Structure from Ray Tracing	167
7.4	Attenuation of Seismic Energy at Broadlands-Ohaaki	179
7.4.1	Attenuation Zones	180
7.4.2	Discussion of Attenuation	183
7.4.3	Attenuation in Volcanic Sequences	186
7.5	Synthetic Seismograms	187
7.6	Correlation of Seismic Profiles with Drill Holes	193
7.6.1	Line 6 and Line 4	193
7.6.2	Line 5 and Line 1	197
7.6.3	Line 2	198

7.6.4	Line 3	201
7.7	Conclusion	202

Chapter 8. Interpretation of Refraction Data over the Broadlands-Ohaaki Geothermal Field

8.1	Introduction	205
8.2	The 1966-68 Broadlands-Ohaaki Seismic Refraction Survey	207
8.3	Reduction of the 1966-68 Refraction Data	211
8.4	Interpretation	213
8.5	Discussion	223
8.6	Summary	225

Chapter 9. Interpretation of Gravity Anomalies over the Broadlands-Ohaaki Geothermal Field

9.1	Introduction	227
9.2	Residual Gravity Anomalies	230
9.3	Density and Porosity Structure	233
9.4	Quantitative Interpretation of Residual Gravity Anomalies	239
9.4.1	Method	239
9.4.2	Results	245
9.5	Summary	260

Chapter 10. Conclusion

10.1	Introduction	263
10.2	Compressional-Wave Velocity and Attenuation in Porous Rocks	264
10.3	Data Acquisition	265
10.4	Data Processing	266
10.5	Interpretation of Shot-Generated Noise	267
10.6	Interpretation of Seismic Reflection Data	268
10.7	Recommendations for Future Seismic Reflection Surveys	269
10.8	Reinterpretation of Seismic Refraction Data	270
10.9	Reinterpretation of Gravity Data	271

Appendix A	Adiabatic Bulk-Modulus of Porous Rocks	277
Appendix B	Attenuation	281
Appendix C	Ray Tracing and Dip Element Computation	289
Appendix D	Gravitational Effect of a $2^{1/2}$ -Dimensional Body	297
Appendix E	Listing of Gravity Station Data	299
Appendix F	Shallow Structure of the Broadlands-Ohaaki Geothermal Field (NZ): Analysis of Seismic Refracted arrivals by iterative ray tracing.	301
Appendix G	Structure of Concealed Igneous Bodies in the Broadlands-Ohaaki Geothermal Field	307
References		315

List of Tables

Table 2.1	Generalised stratigraphy, porosity, mean wet density, and velocities.	18
Table 2.2	Broadlands-Ohaaki geothermal field (1987).	31
Table 3.1	Elastic and thermodynamic properties.	42
Table 4.1	Field parameters for walk-away noise test	59
Table 4.2	Characteristics of major source generated noise events depicted in Figure 4.3.	59
Table 4.3	Maximum migrated dip range for a 20 m group interval using P-wave velocity depth function of Figure 4.9.	70
Table 4.4	Field and recording parameters for seismic reflection measurements.	80
Table 5.1	P-wave velocity versus time function used for spherical divergence correction and Brute Stack...	91
Table 5.2	Deconvolution parameters applied to shot gather records before stacking.	104
Table 5.3	Time variant filter parameters used for post stack enhancement	118
Table 5.4	Normal data processing sequence...	122
Table 9.1	Density and density contrasts of rocks from the Broadlands-Ohaaki geothermal field used for gravity modelling	237

List of Figures

Figure 1.1	Seismic recording geometry and stacking diagram...	3
Figure 2.1	Simplified geology of the Taupo Volcanic Zone (TVZ)...	14
Figure 2.2	Map of the Broadlands-Ohaaki geothermal field...	17
Figure 2.3	Summarised composite of geological and geophysical studies along profile A-A'.	21
Figure 2.4	Summarised composite of geological and geophysical studies along profile B-B'.	22
Figure 2.5	Wet density, particle density, and porosity determinations plotted against depth.	23
Figure 2.6	Perspective block diagram of contoured average wet density and average porosity.	25
Figure 2.7	A plot of seismic P-wave velocity versus bulk density.	27
Figure 2.8	Perspective block diagram of contoured average temperature.	30
Figure 3.1	Adiabatic and isothermal bulk moduli of water...	39
Figure 3.2	P-wave velocities for Huka Falls Formation and the Wairakei Ignimbrite plotted versus temperature.	44
Figure 3.3	Contour plot of relaxed P-wave velocity of Ohaaki Rhyolite as a function porosity and temperature.	44
Figure 3.4	Attenuation as a function of temperature...	44
Figure 3.5	Velocity-depth and attenuation (Q) model of a simple reservoir.	45
Figure 3.6	Synthetic zero-offset section...	45

Figure 3.7	Computed relaxed and unrelaxed P-wave velocities...	48
Figure 3.8	Relaxed P-wave velocity of partially saturated Ohaaki Rhyolite...	48
Figure 3.9	Attenuation for the condition in Figure 3.7.	48
Figure 3.10	Temperature versus depth curve for Br 42.	49
Figure 3.11	Velocity-depth and Q model for a hypothetical two-phase reservoir.	51
Figure 3.12	Synthetic zero-offset section for the model in Figure 3.11	51
Figure 4.1	Comparison of scale...	54
Figure 4.2	Location of seismic reflection test profiles and Walk-away noise spread...	56
Figure 4.3	Display of Walk-away records with trace balancing and AGC...	58
Figure 4.4	Response of an array containing 8 geophones each 5 m apart.	61
Figure 4.5	The effect of dip on total delay across a linear geophone array.	61
Figure 4.6	Time series and amplitude spectrum...	63
Figure 4.7	Comparison of CMP-stacked traces...	64
Figure 4.8	Normalised damped frequency response curve of the single 14 Hz geophone...	65
Figure 4.9	Velocity model ...	67
Figure 4.10	Vertical component synthetic seismograms for the model in Figure 4.9...	68
Figure 4.11	Stretch mute patterns for major reflections shown on Figure 4.10	68

Figure 4.12	Comparison of shot gathers...	72
Figure 4.13	The effect of decreasing depth of shot point at test profile 2...	73
Figure 4.14	Horizontal component theoretical seismogram for the model in Figure 4.9...	75
Figure 4.15	Field records obtained using horizontally aligned geophones and vertical geophones...	76
Figure 4.16	Map of the Broadlands-Ohaaki geothermal field showing the location of seismic reflection profiles.	79
Figure 5.1.	Unprocessed shot gathers...	85
Figure 5.2	Time series and Amplitude spectrum of trace 7 in Shot 126...	86
Figure 5.3	Processing flow chart developed from the analysis of Line 4.	88
Figure 5.4	Shot gather 126 from Figure 5.1...	90
Figure 5.5	Refracted ray paths for a shot and receiver at the earth's surface.	93
Figure 5.6	Reduced time display of the refracted arrivals from 4 shot records.	94
Figure 5.7	Delay times for Line 6...	96
Figure 5.8	Brute stack of Line 4.	97
Figure 5.9	Frequency-wavenumber (ω - k) spectrum of shot gather 126.	98
Figure 5.10	Shot gather 126 after ω - k filtering...	100
Figure 5.11	Frequency-wavenumber spectrum of shot gather 126...	102
Figure 5.12	Shot gather and autocorrelation of record 126 before predictive deconvolution, and after predictive deconvolution...	103

Figure 5.13	Time series and amplitude spectrum of trace 7 from Figure 5.12.	105
Figure 5.14	Panels of 40 traces each displayed after the application of deconvolution parameters.	106
Figure 5.15	Map of Line 4...	108
Figure 5.16	Velocity spectra of CMP 260 from Line 4.	109
Figure 5.17	Part of a constant velocity stack test..	111
Figure 5.18	Four normal moveout (NMO) corrected CMP gathers...	112
Figure 5.19	Preliminary stack of Line 4...	113
Figure 5.20	Velocity spectra of the CMP gather shown in Figure 5.16...	114
Figure 5.21	Final stack of Line 4...	116
Figure 5.22	Migrated stack of Figure 5.21...	117
Figure 5.23	Part of a filter test...	119
Figure 5.24	True amplitude stack of Line 4.	120
Figure 6.1	Common-receiver gathers for 7 shots repeated at Station 284.	126
Figure 6.2	Location map and elevation profile of Walk-away noise spread	129
Figure 6.3	Frequency-wavenumber (ω - k) transform of the Walk-away data	131
Figure 6.4	Slowness-frequency (p - ω) transform of the Walk-away data	132
Figure 6.5	Simplified velocity-depth models for the near-surface structure.	134
Figure 6.6	Rayleigh wave dispersion curves for models NS1 and NS3...	136

Figure 6.7	Amplitude coefficient of reflected and refracted incident P-waves..	137
Figure 6.8	Synthetic seismograms calculated for the model NS1...	138
Figure 6.9	The source spectrum used for finite difference modelling.	141
Figure 6.10	Velocity-depth model for finite difference acoustic-wave synthetic seismograms...	142
Figure 6.11	Synthetic shot gather for the velocity model in Figure 6.10...	142
Figure 6.12	Snapshots of the displacement fields...	144
Figure 6.13	Field record and corresponding synthetic data for the shot taken at Station 190 on Line 4...	145
Figure 6.14	Common receiver gather and corresponding synthetic data for the detector located at Station 190 on Line 4...	146
Figure 6.15	Logarithm plots representing the results of surface-consistent spectral analysis...	148
Figure 6.16	Autocorrelations representing the results of surface-consistent spectral analysis...	150
Figure 6.17	Autocorrelations representing the results of surface-consistent spectral analysis...	152
Figure 6.18	Deconvolution tests...	154
Figure 6.19	CDP-stacked section of Line 4 after surface-consistent filtering...	156
Figure 6.20	CDP-stacked section of Line 4...	157
Figure 7.1	Northeast-southwest profile Line 6.	Folder
Figure 7.2	Northeast-southwest profile Line 4.	Folder

Figure 7.3	Northeast-southwest profile Line 5.	Folder
Figure 7.4	Northeast-southwest profile Line 1.	Folder
Figure 7.5	Southwest-northeast profile Line 2.	Folder
Figure 7.6	Southwest-northeast profile Line 3.	Folder
Figure 7.7	Fence diagram of initial interval velocity model...	168
Figure 7.8	Resolvable thickness, based on the Rayleigh criterion...	172
Figure 7.9	Fresnel zone radii...	172
Figure 7.10	The initial model and computation mesh used for migrating line 1.	174
Figure 7.11	An intermediate result in the ray tracing procedure.	174
Figure 7.12	The final computation mesh...	175
Figure 7.13	Fence diagram of the final interval velocity model...	176
Figure 7.14	Fence diagram of percentage reduction in interval velocity...	178
Figure 7.15	Smoothed amplitude-decay curves...	180
Figure 7.16	Map of the Broadlands-Ohaaki geothermal field...	182
Figure 7.17	Observed and theoretical velocities compressional wave velocities.	184
Figure 7.18	Comparison of true amplitude stacked seismic reflection data near Br 1 with synthetic seismograms computed...	188
Figure 7.19	Detailed portion of Line 2 near Br 32 showing true amplitude stacked data compared to synthetic traces.	190
Figure 7.20	Detailed portion of Line 2 near Br 42 showing true amplitude stacked data compared to synthetic traces.	191

Figure 7.21	Detailed portion of Line 2 near Br 27 showing true amplitude stacked data compared to synthetic traces.	192
Figure 7.22	Final migrated line segments of line 6 and line 4...	195
Figure 7.23	Final migrated line segments of line 5 and line 1...	195
Figure 7.24	Final migrated line segments of line 2 ...	199
Figure 7.25	Final migrated line segments of line 3...	199
Figure 8.1	Map of the Broadlands-Ohaaki geothermal field...	206
Figure 8.2	Coding form...	208
Figure 8.3	Reduced travel time display of near-offset first arrivals from 13 shot records.	210
Figure 8.4	A comparison of receiver delay times for refraction profile D-D' and reflection Line 3.	210
Figure 8.5	D-D' profile.	212
Figure 8.6	C-C' profile.	214
Figure 8.7	P-P' profile.	216
Figure 8.8	A field reflection record (1984 survey) from Line 1...	218
Figure 8.9	B-B' profile.	220
Figure 8.10	A-A' profile.	222
Figure 8.11	Representative velocity-depth models derived from refraction data and reflection data from chapter 7.	224

Figure 9.1	Geology map and residual Bouguer gravity anomaly map of the Broadlands-Ohaaki geothermal field...	229
Figure 9.2	Isodensity map and isoporosity map of the Ohaaki Rhyolite.	232
Figure 9.3	Isodensity map and isoporosity map of the Waiora Formation.	234
Figure 9.4	Isodensity map and isoporosity map of the Rautawiri Breccia.	236
Figure 9.5	Computed gravitational effect over centre of a rectangular body...	238
Figure 9.6	Composite structure of profile A-A' ...	241
Figure 9.7	Composite structure of profile H-H' ...	241
Figure 9.8	Composite structure of profile B-B'...	241
Figure 9.9	Composite structure of profile C-C'...	241
Figure 9.10	Composite structure of profile D-D'...	241
Figure 9.11	Composite structure of profile P-P'...	241
Figure 9.12	Observed, computed Bouguer anomalies, and interpreted $2^{1/2}$ -dimensional section along profile A-A'.	243
Figure 9.13	Observed, computed Bouguer anomalies, and interpreted $2^{1/2}$ -dimensional section along profile H-H'.	243
Figure 9.14	Observed, computed Bouguer anomalies, and interpreted $2^{1/2}$ -dimensional section along profile B-B'.	243
Figure 9.15	Observed, computed Bouguer anomalies, and interpreted $2^{1/2}$ -dimensional section along profile C-C'.	243
Figure 9.16	Observed, computed Bouguer anomalies, and interpreted $2^{1/2}$ -dimensional section along profile D-D'.	243

Figure 9.17	Observed, computed Bouguer anomalies, and interpreted $2^{1/2}$ -dimensional section along profile P-P'.	243
Figure 9.18	Structural contour map of the basement greywacke...	247
Figure 9.19	Isopachs of the Rautawiri Breccia ...	249
Figure 9.20	Isopachs of the Waiora Formation ...	251
Figure 9.21	Isopachs of the Broadlands Dacite...	253
Figure 9.22	Isopachs of the Broadlands Rhyolite...	255
Figure 9.23	Isopachs of the Ohaaki Rhyolite...	257
Figure B.1	Schematic geometry of rock model used in diffusion solution.	284
Figure B.2	Comparison between the standard linear solid (Zener, 1948) and the diffusion solution.	286
Figure B.3	Normalised intrinsic attenuation as a function of frequency...	286
Figure C.1	Coordinate system for triangular element...	290
Figure D.1	Geometric elements for computing the gravitational effect of $2^{1/2}$ -dimensional polygonal body.	298

Contents of Map Pocket

Line 1	Final Stack
Line 2	Final Stack
Line 3	Final Stack
Line 4	Final Stack
Line 4	Migrated Stack
Line 5	Final Stack
Line 6	Final Stack
Line 7	Final Stack
Line 8	Final Stack
Figure 7.1-7.6	